A Transport Solution for Plasma Fluid Equations that Conserves Particles, Momentum, & Energy

E. William DeShazer

May 20, 2021

Abstract

A predictive transport computational model that solves a recently postulated form of the plasma fluid equations [15] that conserves particles, momentum, and energy will be implemented. The transport equations set will be extended and modified as necessary to provide reasonable agreement with experimental data collected from DIII-D, a research tokamak owned by General Atomics. Thus, a validation exercise comparing against a variety of H-mode, L-Mode and RMP data sets is anticipated in the development of the computational model. The transport equations were proposed to capture the radial distribution resulting from a neutral beam source, which inserts particles, momentum, and energy, ion orbit loss, which removes particles and their associated momentum and energy in a non-diffusive manner, and the equilibrium field conditions of toroidal and poloidal rotation velocities, plasma pressure, density, and temperature. The equations as presented are first order, coupled, non-linear equations, resulting from the long range Lorentz forces $\left(\vec{V} \times \vec{B}\right)$ and electric field $\left(\vec{E}\right)$. Therefore, iterative computational techniques will be employed. The primary solver that will be explored is a variant of the Newton-Raphson multivariate solver known as Broyden's method. A pure Newton-Raphson solver evaluates the Jacobian analytically, but the nature of our equations will require a numerical approximation of the Jacobian. In the course of the analysis if other iterative techniques arise, we will consider implementing them for comparison.

1 Introduction

The path toward fusion as an energy source hinges on an understanding and description of the plasma dynamics. On the experimental side, great effort is being given to access and exploit high performance operational regimes such as H-Mode[7], SH-Mode[5] (Figure 1a on page 2) and the most recent addition, NT-Mode[10, 11] (Figure 1b on page 2). Each of these regimes show improved plasma performance characteristics in the form of longer confinement times, but many codes, including SOLPS, UEDGE, or ONETWO, satisfy fluid conservation equations in the absence of electromagnetic effects. Instead these codes assume diffusion as the primary transport mechanism and impose electromagnetic effects after the equilibrium field has been solved. One of the key weaknesses in this modeling approach is diffusion implies that particles move down the pressure gradient, whereas the aforementioned regimes should exhibit increased transport in the presence of steep pressure gradients at the plasma edge. In fact, they exhibit exactly the opposite.

Within the plasma community it is known that the exhibited improved performance implies a pinch effect, but a satisfying descriptive model to explain these effects has been elusive. The fluid equations as proposed by Stacey [15] and outlined in Section 2 has the pleasing feature that the long-range $\vec{V} \times \vec{B}$ forces are retained in the momentum conservation equations Section 2.3 while introducing a more theoretically sound mechanism for particle loss in the form of Ion Orbit Loss (IOL), both thermal and fast.

The justification that IOL is more theoretically sound arises from the observation that diffusion, a near-field

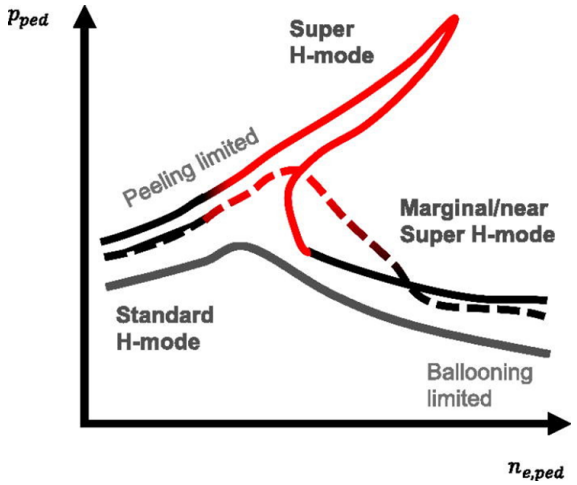

(a) Pedestal Bifurcation during Super H-Mode in Density Space [5]

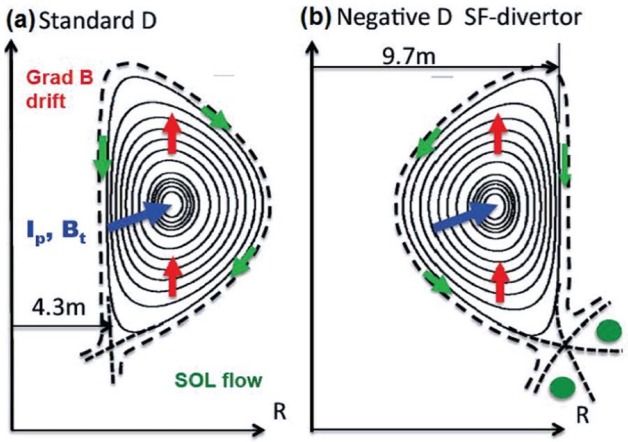

(b) Equilibrium configurations and Scrape-off Layer (SOL) flow patterns for (a) standard D-shaped tokamak and (b) negative triangularity snowflake divertor tokamak [11]

Figure 1: High Performance Operational Regimes

effect that is driven by pressure gradients, is an inherently collisional transport mechanism. However, central to the theory of a plasma is that it is most assuredly not. The IOL argument is that the particles within a flux surface, to a first order, satisfy conservation canonical angular momentum, energy, and magnetic moment, as will be discussed in Section 2.2. The flux surface energy, in the form of temperature, is a Maxwellian distribution, which means particles in the tail, have sufficient energy to take particles beyond the Last Closed Flux Surface (LCFS). Both magnetic field irregularities and physical barriers, such as walls, result in particles being removed while trying to execute orbits.

The inclusion of long-range $\vec{V} \times \vec{B}$ forces into the momentum conservation as discussed in Section 2.3 is satisfying because it forces the equilibrium solution for the pressure field to re-balance in the presence of the fluid velocities, both the toroidal, V_ψ, and poloidal, V_θ.

The fluid theory presented in this paper has developed in some form at the Georgia Institute of Technology (GIT) Fusion Research Center (FRC) for as long as fusion has been actively researched there. However, the effort to fully describe the physics in the edge and pedestal region were outlined in "A framework for the development and testing of an edge pedestal model: Formulation and initial comparison with DIII-D data"[18]. Stacey and Groebner lay out the physics constraints that are important to an plasma edge/pedestal model in Section II and detail a road-map on the work required realize the ultimate goal stated in Section VI, a fully predictive pedestal model.

The formal statement of this fluid theory appears first in "Edge pedestal structure" from Stacey[14]. Many of the modeling assumptions, such as the observation that a phase space integration of the generalized continuity equation results in only a radially flux or the form of the effective diffusion coefficient, are presented. In a series of several papers, [16, 21, 2, 28], the transport formalism that is being studied in this paper was used to interpret particle flux, IOL, and intrinsic rotation based on experimental input of density and temperature. In fact, the model was shown to have an agreement with experimental rotation velocity data from DIII-D to within 10-20%[21].

The next step, and the objective of this research, is the final step of the 2003 paper [18] is to produce a predictive transport model that conserves particles, momentum and energy by including the non-diffusive loss mechanism of IOL and retaining the long range electromagnetic contributions of $\vec{V} \times \vec{B}$. A necessary and intermediate step is to provide an iterative computational algorithm that is compatible with the strong E&M and $\vec{V} \times \vec{B}$ forces simultaneously with the weaker scattering forces. To this end, we will explore the

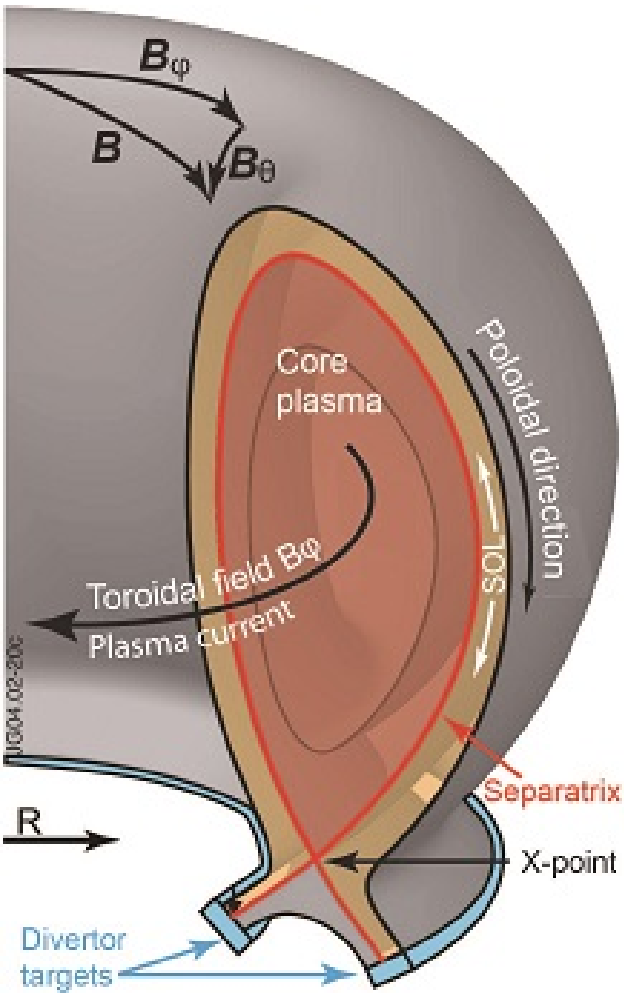

Figure 2

Broyden algorithm, a quasi Newton-Raphson method, as the primary iterative solver in combination with Gauss reduction. A validation exercise against a variety of operational modes, L-Mode, H-Mode, NT-Mode, and Reverse Magnetic Pinch (RMP) is envisioned. The result will be a code that predicts the radial density, pressure, and temperature fields as well as the associated toroidal and poloidal velocities.

1.1 Regions of a Tokamak Plasma

High level features of a tokamak plasma are illustrated in the Figure 2 on page 3. These regions include the Core Plasma, the Scrape-off Layer (SOL), which will sometimes be referred to as the edge region, the Separatrix, which will also be referred to as the Last Closed Flux Surface (LCFS), and the X-Point, which is a feature of a divertor design. Also illustrated in this figure is the major radius, R, which is measured from the central axis of the torus. The toroidal direction, φ, and the poloidal direction are represented. In accordance with these directions, the magnetic field $\vec{B}$ is decomposed into a direction aligned with the toroidal direction, $\vec{B}_{\varphi}$ and a component that is in the poloidal direction, $\vec{B}_{\theta}$. Velocity can be decomposed as either parallel to $\vec{B}$, $\left(V_{\parallel}\right)$, perpendicular to $\vec{B}$, $(V_{\perp})$ or along one of the toroidal directions $\left(V_{\varphi}\right.$ or $\left.V_{\Theta}\right)$. The minor axis, r, which is not illustrated here, extends from the plasma magnetic center to the outer wall. For this reason, the radius that works its way into equations is not a fixed value but is given by Equation (1)

$$R\left(r\right) = R_0 + r\cos\theta \tag{1}$$

where, R_0 is the radial distance from toroidal center to the magnetic center. Because, this analytical approach is one-dimensional $\theta = 0$ and $R(r)$ is simply $R_0 + r$

2 Theory

The fundamental parts of the predictive model are the conservation of particles (Section 2.1), momentum (Section 2.3), and energy (Section 2.4), the conduction closure (Section 2.5) and the ideal gas law (Section 2.7). Within each of the conservation equations there is provision for the removal of particles, momentum, and energy due to IOL, which is described in Section 2.2. IOL calculation requires input from the equilibrium reconstruction. Therefore, a short overview is provided in Section 2.5.3. The primary source of particles, momentum, and energy considered is beam input and therefore, details on the beam modeling are covered in Section 2.6. Finally, the pinch diffusion model is described, because there is a desire to recast the conservation equations in the form of a pinch diffusion equation. Therefore, the pinch diffusion model will be discussed in Section 2.8

2.1 Conservation of Particles

The general multidimensional form of the continuity equation in Equation (2)

$$\boldsymbol{\nabla} \cdot n_j \mathbf{v}_j = S_j \tag{2}$$

reduces to the one-dimensional non-linear Ordinary Differential Equation (ODE) shown in Equation (3) and Equation (4) when one performs a Flux Surface Average (FSA). The reason is that the poloidal component of the flux, $\langle \left(\boldsymbol{\nabla} \cdot n_j \mathbf{v}_j\right)_\theta \rangle = 0$ identically and $\langle \left(\boldsymbol{\nabla} \cdot n_j \mathbf{v}_j\right)_\phi \rangle = 0$ by axisymmetry [14].

$$\frac{1}{r}\frac{\partial}{\partial r}\Big(r\Gamma_{rj}(r)\Big) = S_{nj} - \alpha\frac{\partial}{\partial r}\Big(F_j^{\text{iol}}(r)\Big)\Gamma_{rj}(r) - \beta z_k \frac{\partial}{\partial r}\Big(F_k^{\text{iol}}\left(r\right)\Big)\Gamma_{rk}(r) \tag{3}$$

where,

$$S_{nj} \equiv N_{\text{nbj}}(r)\left(1 \ -\hat{\alpha} f_{\text{nbi}}^{\text{iol}}(r)\right) + n_e(r)\,\nu_{\text{ion}_j}(r) \tag{4}$$

The left side of Equation (3) expresses the change in flux, Γ_{rj} of the primary ion is driven by the source terms on the right. First, S_{nj}, is the positive contributions due to Neutral Beam Injection (NBI) and ionization. In Equation (4), N_{nbj} is the rate of NBI injection, which has been reduced by the fast IOL, $f_{\text{nbi}}^{\text{iol}}$. The rate of neutral beam injection is based on a beam model that is described in Section 2.6. The second term, $n_e(r)\,\nu_{\text{ion}_j}(r)$ is the ionization rate and is discussed in Section 2.9. Lastly, in Equation (3), there are two terms for IOL, $F_j^{\text{iol}}(r)$ for the primary ion, and $F_k^{\text{iol}}\left(r\right)$ for the impurity ion. They are the cumulative loss of ions through the mechanism of IOL. They impact the conservation of particles through their differential contributions, $\frac{\partial}{\partial r}$. These IOL terms are detailed in Section 2.2. The terms, α and β are charge neutrality adjustment terms and will be a subject of consideration. There are three mechanisms by which the charge associated with lost primary ions can be compensated:

(i) A commensurate lost electrons implying ($\alpha = 1, \beta = 0$) thus nullifying $F_k^{\text{iol}}\left(r\right)$,

(ii) A return current of thermalized ions from the SOL (SOL) implying ($\alpha = 2, \beta = 1$), or

(iii) No IOL ($\alpha = 0, \beta = 0$)

Stacey conjectures that the most physically reasonable is item (ii), which we intend to explore.

2.2 Ion Orbit Loss

Ion Orbit Loss (IOL) represents a non-diffusive mechanism for losing particles. At the heart of IOL theory is an electromagnetic equilibrium argument that, to a first order, between any two flux surfaces canonical angular momentum (Equation (5)), energy (Equation (6)), and magnetic moment (Equation (7)) are

conserved. Based on this fundamental principle, Miyamoto [12] observed that one could use the values of plasma parameters on an inner flux surface (marked with a subscript 0) and the parameters on a separatrix, (marked with a subscript s or no subscript). Figure 2 on page 3 illustrates two flux surfaces, one being the separatrix and an inner one between the core and edge region.

$$\left[R\, m\, V_{\parallel} \left(\frac{B_{\varphi}}{B} \right) + e\psi \right]_0 = \left[R\, m\, V_{\parallel} \left(\frac{B_{\varphi}}{B} \right) + e\psi \right]_s \tag{5}$$

$$\left[\frac{1}{2} \left(V_{\parallel}^2 + V_{\perp}^2 \right) \right]_0 = \left[\frac{1}{2} \left(V_{\parallel}^2 + V_{\perp}^2 \right) \right]_s \tag{6}$$

$$\left[\frac{m\, V_{\perp}^2}{2\, B} \right]_0 = \left[\frac{m\, V_{\perp}^2}{2\, B} \right]_s \tag{7}$$

Utilizing Equation (8), defining the term f_{φ} in Equation (9) and the parameter ζ_0, which is the direction cosine of the particles launch angle with respect to the toroidal magnetic field line, B_{φ}, Equations (5) to (7) can be rewritten into Equation (11). This equation, which is quadratic in V_0, represents the equilibrium velocity for a particle to have an orbit that is within the confined portion of the plasma, meaning within the separatrix.

$$V_0 = \sqrt{V_{\parallel}^2 + V_{\perp}^2} \tag{8}$$

$$f_{\varphi} = \left| \frac{B_{\varphi}}{B} \right| \tag{9}$$

$$\zeta_0 = \frac{V_{\parallel 0}}{V_0} \tag{10}$$

This then serves as the criterion for which a particle can be lost. If it has an energy in excess of this, then it will have an orbit outside of the confined plasma and can encounter a variety of obstructions, such as magnetic field imperfections, SOL particles, and most obviously, the wall. The manner by which this minimum velocity is applied to calculate a loss estimate is described in Section 2.2.1.

$$\begin{aligned} V_0^2 \left[\left(\frac{R_0}{R} \frac{f_{\varphi 0}}{f_{\varphi}} \zeta_0 \right)^2 - 1 + (1 - \zeta_0^2) \left| \frac{B}{B_0} \right| \right] + V_0 \left[\frac{2e\,(\psi_0 - \psi)}{R m f_{\varphi}} \left(\frac{R_0}{R} \frac{f_{\varphi 0}}{f_{\varphi}} \zeta_0 \right) \right] \\ + \left[\left(\frac{e\,(\psi_0 - \psi)}{R m f_{\varphi}} \right)^2 - \frac{2e\,(\phi_0 - \phi)}{m} \right] = 0 \end{aligned} \tag{11}$$

Figure 3 on page 6 shows the minimum energy calculations against plasma ion temperature, what this illustrates is that IOL is not a dominant transport mechanism for the plasma core. However, it becomes the dominant effect in the last 5% [22] and drives the features in this region.

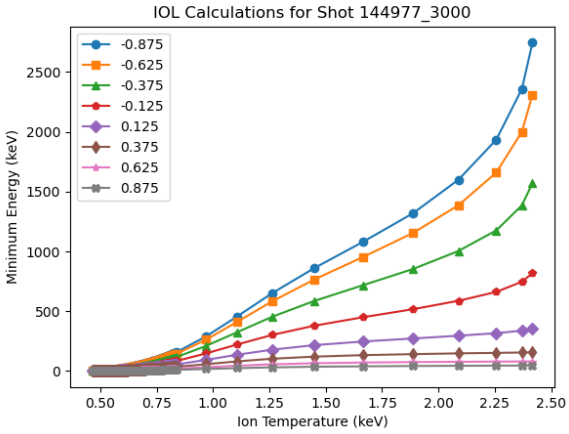

Figure 3: Minimum Energy calculation for Shot 144977.3000

2.2.1 Cumulative Loss Fraction

The temperature of any flux surface is assumed to be Maxwellian in the velocity space, which means that if one assumes a three dimensional velocity space, the distribution of energy is given by a Gamma distribution as illustrated in Figure 4a on page 6. The cumulative loss fraction, F_{rj}^{IOL}, is determined by truncating the distribution above the minimum energy given in Equation (12). This leads to an evaluation of the incomplete Gamma distribution, Γ, at $\epsilon(\rho, \zeta_0)$. The zeroth moment, which corresponds to particle loss, results in a $\Gamma\left(\frac{3}{2}\right)$ shown in Equation (13). The first moment, which corresponds to momentum loss, results in $\Gamma(2)$ shown in Equation (14). The second moment, which corresponds to energy loss, results in $\Gamma\left(\frac{5}{2}\right)$ shown in Equation (15).

$$\epsilon_{min} = \frac{1}{2} m V_0^2 \tag{12}$$

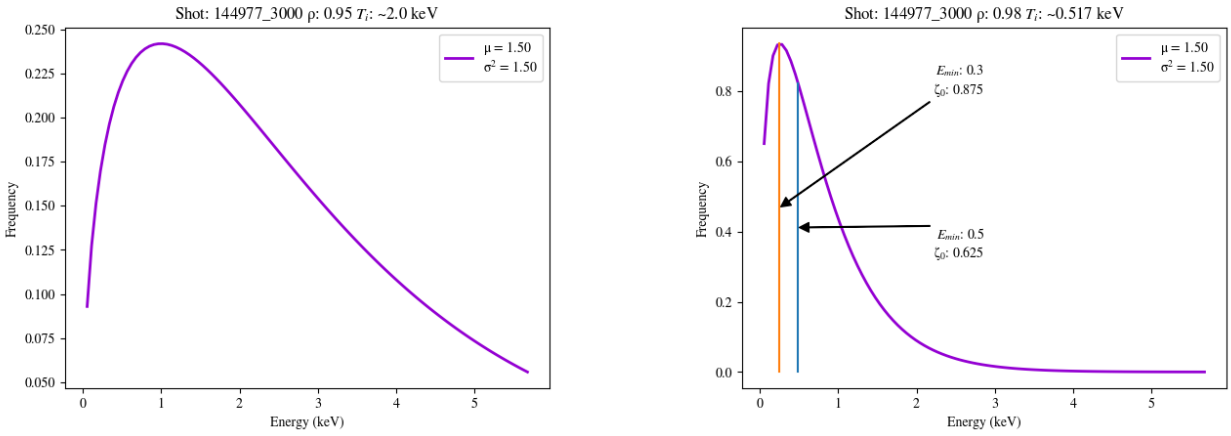

(a) Core Region

(b) $\rho = 0.98$, $T_i = 0.517keV$

Figure 4: Maxwellian Gamma Distribution for shot 144977.3000

One aspect of the IOL that is important to note is that the equilibrium given by Equations (5) to (7) identify which particles have energy that take them beyond the LCFS, but this does not necessarily imply

loss. Instead it implies a sufficient orbit to enter unfavorable zones. From this observation, one has to postulate that a certain number of these particles will either i) suffer a collision in the SOL, which is not collisionless and therefore reasonable, or ii) particles strike the wall. With this in mind, we utilize the Stacey rational approximation that R_{loss}^{IOL} is approximately 0.5, the logic being that some is more likely than none, while all is probably too much. Half is about right.

$$F_{rj}^{IOL}(r) = \frac{N_{loss}}{N_{total}} = \frac{R_{loss}^{IOL}\int_{-1}^{1}\left[\int_{V_{0,min}}^{\infty} V_0^2 f(V_0)\, dV_0\right] d\zeta_0}{2\int_0^{\infty} V_0^2 f(V_0)\, dV_0} = \frac{R_{loss}^{IOL}\int_{-1}^{1} \mathbb{\Gamma}\left(\frac{3}{2}, \epsilon_{min}(\rho,\zeta_0)\right) d\zeta_0}{2\mathbb{\Gamma}\left(\frac{3}{2}\right)} \tag{13}$$

$$M_{rj}^{IOL}(r) = \frac{M_{loss}}{M_{total}} = \frac{R_{loss}^{IOL}\int_{-1}^{1}\left[\int_{V_{0,min}}^{\infty} (m\,V_0\,\zeta_0)\, V_0^2 f(V_0)\, dV_0\right] d\zeta_0}{2\int_0^{\infty} (m\,V_0)\, V_0^2 f(V_0)\, dV_0} = \frac{R_{loss}^{IOL}\int_{-1}^{1} \mathbb{\Gamma}(2, \epsilon_{min}(\rho,\zeta_0))\, d\zeta_0}{2\mathbb{\Gamma}(2)} \tag{14}$$

$$E_{rj}^{IOL}(r) = \frac{E_{loss}}{E_{total}} = \frac{R_{loss}^{IOL}\int_{-1}^{1}\left[\int_{V_{0,min}}^{\infty} \left(\frac{1}{2} m\, V_0^2\right) V_0^2 f(V_0)\, dV_0\right] d\zeta_0}{2\int_0^{\infty} \left(\frac{1}{2} m\, V_0^2\, \zeta_0\right) V_0^2 f(V_0)\, dV_0} = \frac{R_{loss}^{IOL}\int_{-1}^{1} \mathbb{\Gamma}\left(\frac{5}{2}, \epsilon_{min}(\rho,\zeta_0)\right) d\zeta_0}{2\mathbb{\Gamma}\left(\frac{5}{2}\right)} \tag{15}$$

2.3 Conservation of Momentum

A very important aspect of the equations utilized for this research is that the momentum conservation recovers the fundamental electromagnetic principle inherent in the Lorentz $\vec{V} \times \vec{B}$ forces, which are orthogonal to the direction of motion.

$$\vec{F} = e(\vec{E} + \vec{V} \times \vec{B}) \tag{16}$$

For this reason the bulk fluid toroidal, V_φ, and poloidal V_θ velocities influence the radial momentum conservation in Section 2.3.1 and the poloidal in Section 2.3.3. Additionally, because there is a radial particle flux outward, Γ_{rj}, Γ_{rk}, there is a radial electric field that manifests.

2.3.1 Radial

The radial momentum equates the normal force of pressure gradient with the orthogonal contribution of the $\vec{V} \times \vec{B}$. A technique to recapture the pressure is to utilize the gradient scale length (Equation (17)). It is an empirically derived parameter that is determined from a form of the equations that we are solving [17] and represents a fundamental property in the plasma edge. In the radial direction, the $\vec{V} \times \vec{B}$ terms that contribute to the force balance are the $eV_\theta\, B_\varphi$ and the e

$$L_p^{-1} \equiv= \frac{1}{p}\frac{\partial p}{\partial r} \tag{17}$$

$$\begin{bmatrix} p_j L_{p_j}^{-1} \\ p_k L_{p_k}^{-1} \end{bmatrix} = \begin{bmatrix} -\dfrac{1}{1+\dfrac{z_j}{z_k}\dfrac{n_j}{n_k}} & \dfrac{1}{1+\dfrac{z_k}{z_j}\dfrac{n_k}{n_j}} \\ \dfrac{1}{1+\dfrac{z_k}{z_k}\dfrac{n_j}{n_k}} & -\dfrac{1}{\dfrac{n_k}{n_j}\dfrac{z_k}{z_j}+1} \end{bmatrix}^{-1} \begin{bmatrix} \dfrac{n_j z_j}{1+\dfrac{n_j}{n_k}\dfrac{m_j}{m_k}} & \dfrac{n_j z_j}{1+\dfrac{n_j}{n_k}\dfrac{m_j}{m_k}} \\ \dfrac{n_k z_k}{1+\dfrac{n_k}{n_j}\dfrac{m_k}{m_j}} & \dfrac{n_j z_j}{1+\dfrac{n_k}{n_j}\dfrac{m_k}{m_j}} \end{bmatrix} \left[eB_\varphi \begin{bmatrix} V_{\theta j} \\ V_{\theta k} \end{bmatrix} - eB_\theta \begin{bmatrix} V_{\varphi j} \\ V_{\varphi k} \end{bmatrix} \right] \tag{18}$$

2.3.2 Toroidal

The toroidal momentum balance expressed in Equation (19) equates the forces due to the fluid velocity, V_φ, with the force due to the toroidal electric field, E_φ^A, the Lorentz force associated with a radial flux, the momentum input of NBI and finally the momentum loss due to IOL. It is of some value to deconstruct several of the terms to gain an intuition for these terms.

- The force associated with the fluid velocity arises from two physical considerations, collisional drag within the species expressed as a frequency, ν_{dj}, and inter-species drag, ν_{jk}. As an aside it helped the author to do a units analysis that this works to force per unit volume.
- The electric field E_φ^A is simply a result of current drive and is therefore an externally applied condition.
- the $e\,B_\theta\Gamma$ term is a masked Lorentz force. The flux is motion of the charged ionized particles, which produce an orthogonal force as they move across a magnetic field line.
- The momentum of the IOL term is due to an instantaneous loss of particles. The model description is given in Equation (14)

$$\begin{bmatrix} n_j m_j \left(\nu_{jk} + \nu_{dj}^\varphi\right) & -n_j m_j \nu_{jk} \\ -n_k m_k \nu_{kj} & n_k m_k \left(\nu_{kj} + \nu_{dk}^\varphi\right) \end{bmatrix} \begin{bmatrix} \hat{V}_{\varphi j}(r) \\ \hat{V}_{\varphi k}(r) \end{bmatrix} = \begin{bmatrix} n_j e_j \\ n_k e_k \end{bmatrix} E_\varphi^A + \begin{bmatrix} e_j B_\theta & 0 \\ 0 & e_k B_\theta \end{bmatrix} \begin{bmatrix} \Gamma_{rj}(r) \\ \Gamma_{rk}(r) \end{bmatrix} + \begin{bmatrix} M_{\varphi j}^{\mathrm{nbi}}(r) \\ M_{\varphi k}^{\mathrm{nbi}}(r) \end{bmatrix} - \begin{bmatrix} M_{\varphi j}^{\mathrm{iol}}(r) \\ M_{\varphi k}^{\mathrm{iol}}(r) \end{bmatrix} \tag{19}$$

2.3.3 Poloidal

The poloidal momentum conservation is described by Equation (20). Most of the terms in the poloidal momentum balance are the same as the toroidal momentum balance, which is explained in Section 2.3.2, but the appropriate changes for the orthogonal Lorentz contributions. The third time on the right of Equation (20), however, is unique. It results from the gyro-viscous considerations that are negligible in a straight cylindrical plasma, as modeled by Braginskii[[1]], but are significant in a toroidally confined plasma, due to the curvature of the field lines [26]. The coefficient, K, is the Stacey-Sigmar coefficients which can be found in "Viscous effects in a collisional tokamak plasma with strong rotation" [20].

$$\begin{bmatrix} n_j m_j \left(\nu_{jk} + \nu_{dj}^\theta\right) & -n_j m_j \nu_{jk} \\ -n_k m_k \nu_{kj} & n_k m_k \left(\nu_{kj} + \nu_{dk}^\theta\right) \end{bmatrix} \begin{bmatrix} \hat{V}_{\theta j}(r) \\ \hat{V}_{\theta k}(r) \end{bmatrix} = \begin{bmatrix} n_j e_j \\ n_k e_k \end{bmatrix} E_\theta^A + \begin{bmatrix} e_j B_\phi & 0 \\ 0 & e_k B_\phi \end{bmatrix} \begin{bmatrix} \Gamma_{rj}(r) \\ \Gamma_{rk}(r) \end{bmatrix} + \frac{B_\phi}{B^2} \begin{bmatrix} \nu_{dj}^\theta \dfrac{K_j}{e_j} & 0 \\ 0 & \nu_{dk}^\theta \dfrac{K_k}{e_k} \end{bmatrix} \begin{bmatrix} L_{T_j}^{-1} \\ L_{T_k}^{-1} \end{bmatrix} + \begin{bmatrix} M_{\theta j}^{\mathrm{nbi}}(r) \\ M_{\theta k}^{\mathrm{nbi}}(r) \end{bmatrix} - \begin{bmatrix} M_{\theta j}^{\mathrm{iol}}(r) \\ M_{\theta k}^{\mathrm{iol}}(r) \end{bmatrix} \tag{20}$$

2.4 Conservation of Energy

There are conservation considerations for both the primary ion Equation (21) and electron Equation (22). Both equations are roughly the same. They are both one-dimensional non-linear radial partial differential equations. There is consideration for beam heating(q_{nbi}), fast ion orbit loss (e^{iol}_{nbi}), and ion-electron (q_{re}) and ion-impurity (q_{jk}) cross heating through scattering. Unique aspects of each are discussed in their subsections. It should be noted that other heat sources can be included, but these are considered the primary heat mechanisms at the moment.

2.4.1 Ion Radial Heat Flux

A unique aspect to the ion radial heat flux (Equation (21)) is that there is consideration for charge exchange, $\langle \sigma v \rangle$ between impurity ions and the primary ion. Also, only the ions experience thermal IOL.

$$\frac{1}{r}\frac{\partial\left(r\hat{Q}_{rj}(r)\right)}{\partial r} = q_j^{\mathrm{nbi}}(r)\left(1-\hat{\alpha}e_{\mathrm{nbi}}^{\mathrm{iol}}(r)\right) - q_{je}(r) - q_{jk} \\ - n_j(r)n_{oj}(r)\langle\sigma v\rangle_{\mathrm{cx}}\left(\hat{T}_j(r)-T_{oj}\right) - \frac{\partial E_j^{\mathrm{iol}}(r)}{\partial r}\hat{Q}_{rj}(r) \tag{21}$$

2.4.2 Electron Radial Heat Flux

For the electron heat equation, there is unique consideration for the radiation emissivity, L.

$$\frac{1}{r}\frac{\partial\left(r\hat{Q}_{re}(r)\right)}{\partial r} = q_e^{\mathrm{nbi}}(r) - q_{je}(r) - q_{ke} \\ - n_j(r)n_{oj}(r)\langle\sigma v\rangle_{\mathrm{ionj}}E_{\mathrm{ionj}} - n_k(r)n_{ok}(r)\langle\sigma v\rangle_{\mathrm{ionk}}E_{\mathrm{ionk}} - n_e n_j L_j(r) - n_e n_k L_k(r) \tag{22}$$

2.5 Conduction Closure Equations

As is always the case with the first three moment equations, there is an issue of closure. For this model, we utilize the ion (Equation (23)) and electron conduction (Equation (24)) closure equations. Both are based on a Fick's law model of heat conduction with a conduction coefficient χ. The radial gradient of heat is proportional to the total heat on sources on the right side. Both models share a total heat term Q_j, Q_e which has been adjusted by a convection like term $\frac{5}{2}T\,\Gamma$, which represents the energy associated with the particles that have been lost. The only unique feature is that the ion conduction equation has a term for the total viscous heat loss and the heat stored in the form of rotation.

2.5.1 Ion Conduction

$$-n_i\chi_j\left(\frac{1}{r}\frac{\partial}{\partial r}\left(rT_j(r)\right)\right) \equiv n_j\chi_j T_j(r)L_{T_j}^{-1} = q_j(r) = Q_j(r) - \frac{5}{2}T_j(r)\,\Gamma_{rj}(r) - Q_{\mathrm{vis}_j}(r) - Q_{\mathrm{rot}_j}(r) \tag{23}$$

2.5.2 Electron Conduction

$$-n_e\chi_e\left(\frac{1}{r}\frac{\partial}{\partial r}\left(rT_e(r)\right)\right) \equiv n_e\chi_e T_e(r)\,L_{T_e}^{-1} = q_e(r) = Q_e(r) - \frac{5}{2}T_e(r)\,\Gamma_{re}(r) \tag{24}$$

2.5.3 Equilibrium Reconstruction

A primary input into the IOL model is the flux surface ψ (see Equation (11)). ψ is a parameter that quantifies the amount of enclosed magnetic field. One issue that must determined is the magnetic field topology, both shape and location, which is referred to as MHD equilibrium reconstruction. It is based on solving the Grad-Shafronov equations (Equation (25) and Equation (26)). The work horse tool that performs this reconstruction is EFIT [6]. It balances the magnetic field forces with toroidal current density, i.e. plasma pressure and Lorentz forces due to poloidal field currents. For this research, the flux surfaces from the MHD reconstruction will be considered as defined.

$$\Delta * (\psi) = \mu_0 R J_T \tag{25}$$

$$J_T = R \left[P' (\psi; \alpha_n) + \frac{\mu_0 F F' (\psi; \gamma_n)}{4\pi^2 R^2} \right] \tag{26}$$

2.6 Beam Modeling

The beam model that will be utilized was developed by Mandrekas [9] for the "SuperCode". The model is based on a detailed quantum physics analysis to construct the cross-sections, but the implementation was simplified to a fit in Equation (27) based on the parameters:

- Beam Energy, E in keV/u,
- Beam particle atomic number, u
- Plasma Z-effective, Z_{eff}
- Electron Temperature, T_e in keV, and
- Ion density, n_e in cm^{-3}.

The primary cross-section function, S_1, is determined using Equation (28) and the coefficients Table 1a. Similarly, the impurity cross-section function, S_z is calculated Equation (29) with coefficients being shown in Table 1b. The sensitivity of the cross-section temperature for $Z_{eff} = 1$ and $Z_{eff} = 2$ are shown in Figure 5a on page 11 and Figure 5b on page 11, respectively. The sensitivity due to density is for the same Z_{eff} are presented in Figure 6a on page 12 and Figure 6b on page 12.

The dominant physics for the beam energies, plasma densities and temperatures for tokamak plasmas are collisional radiative [3].

$$\sigma_s^{(z)} \left(E, n_e, T_e, Z_{eff} \right) = \frac{\exp \left[S_1 \left(E, n_e, T_e \right) \right]}{E} \times \left[1 + \left(Z_{eff} - 1 \right) S_z \left(E, n_e, T_e \right) \right] \left(\times 10^{-16} \text{cm}^2 \right) \tag{27}$$

where

$$S_1 = \sum_{i=1}^{2} \sum_{j=1}^{3} \sum_{k=1}^{2} \left\{ A_{ijk} \times \left(\ln E \right)^{i-1} \left[\ln \left(\frac{n}{n_0} \right) \right]^{j-1} \left(\ln T_e \right)^{k-1} \right\} \tag{28}$$

and

$$S_z = \sum_{i=1}^{3} \sum_{j=1}^{2} \sum_{k=1}^{2} \left\{ B_{ijk}^{(z)} \times \left(\ln E \right)^{i-1} \left[\ln \left(\frac{n}{n_0} \right) \right]^{j-1} \left(\ln T_e \right)^{k-1} \right\} \tag{29}$$

Table 1: Values of fit coefficients[3]

(a) A_{ijk} coefficients Equation (28)

A_{ijk}	
A_{111}	4.40
A_{112}	-2.49×10^{-2}
A_{121}	7.46×10^{-2}
A_{122}	2.27×10^{-3}
A_{131}	3.16×10^{-3}
A_{132}	-2.78×10^{-5}
A_{211}	2.30×10^{-1}
A_{212}	-1.15×10^{-2}
A_{221}	-2.55×10^{-3}
A_{222}	-6.20×10^{-4}
A_{231}	-1.32×10^{-3}

(b) B_{ijk} coefficients for He, C, O and Fe Impurities Equation (29)

$B_{ijk}^{(z)}$	He	C	O	Fe
B_{111}	-2.36×10^{0}	-1.49×10^{0}	-1.41×10^{0}	-1.03×10^{0}
B_{112}	1.85×10^{-1}	-1.54×10^{-2}	-4.08×10^{-4}	1.06×10^{-1}
B_{121}	-2.50×10^{-1}	-1.19×10^{-1}	-1.08×10^{-1}	-5.58×10^{-2}
B_{122}	-3.81×10^{-2}	-1.50×10^{-2}	-1.38×10^{-2}	-3.72×10^{-3}
B_{211}	8.49×10^{-1}	5.18×10^{-1}	4.77×10^{-1}	3.22×10^{-1}
B_{212}	-4.78×10^{-2}	7.18×10^{-3}	1.57×10^{-3}	-3.75×10^{-2}
B_{221}	6.77×10^{-2}	2.92×10^{-2}	2.59×10^{-2}	1.24×10^{-2}
B_{222}	1.05×10^{-2}	3.66×10^{-3}	3.33×10^{-3}	8.61×10^{-4}
B_{311}	-5.88×10^{-2}	-3.36×10^{-2}	-3.05×10^{-2}	-1.87×10^{-2}
B_{312}	4.34×10^{-3}	3.41×10^{-4}	7.35×10^{-4}	3.53×10^{-3}
B_{321}	-4.48×10^{-3}	-1.79×10^{-3}	-1.57×10^{-3}	-7.43×10^{-4}
B_{322}	-6.76×10^{-4}	-2.04×10^{-4}	-1.86×10^{-4}	-5.12×10^{-5}

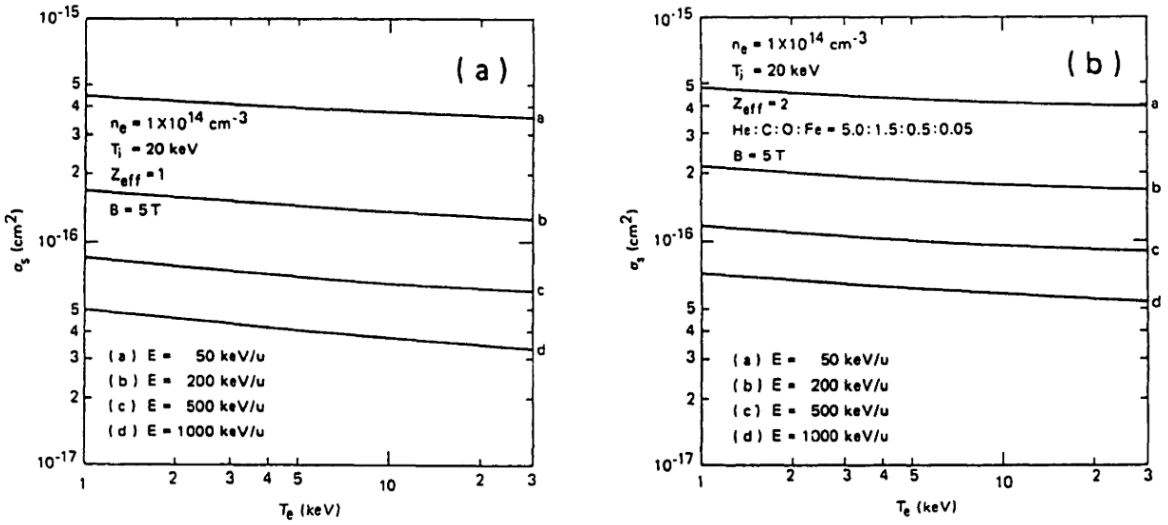

(a) $Z_{eff} = 1$ (b) $Z_{eff} = 2$

Figure 5: Temperature dependence of σ_s for $n_e = 10^{14}$ cm^{-3} for several beam energies [3]

2.7 Ideal Gas Law

The relationship between the pressure calculated in the momentum equation and the density that initializes the iteration, there is an implied temperature which is given by the ideal gas law

$$P = n\,T \tag{30}$$

Based on the iteration strategy chosen (Section 3), this temperature must align with the temperature implied by conservation of energy.

2.8 Pinch Diffusion

It is hoped that this research will culminate with an easy way to reincorporate the $\vec{V} \times \vec{B}$ and IOL physics into traditional diffusion models. In [24], Stacey provides a diffusion-like model that has a Γ^{Pinch} term

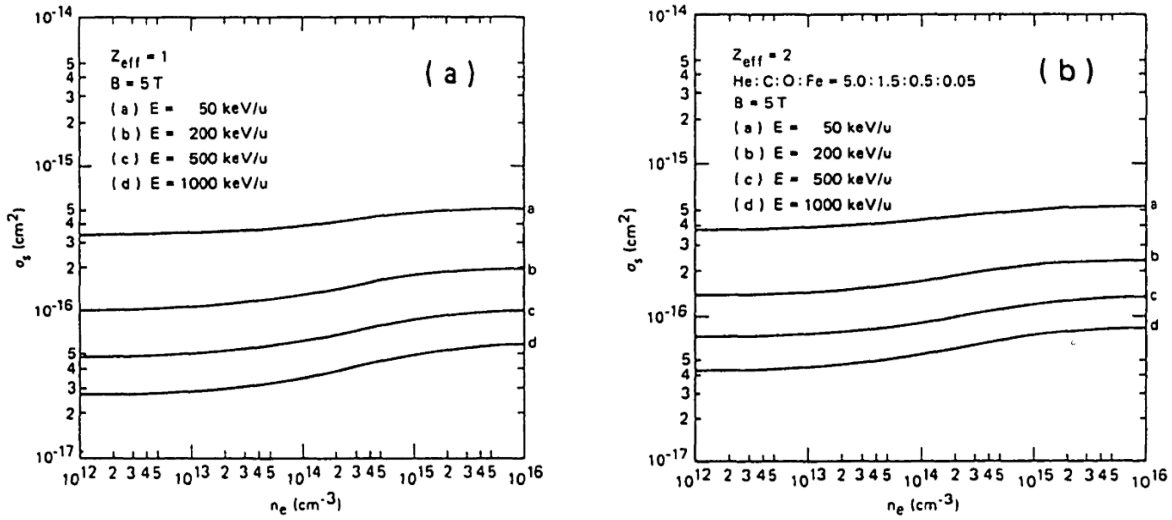

(a) $Z_{eff} = 1$ (b) $Z_{eff} = 2$

Figure 6: Density dependence of σ_s for several beam energies [3]

that retains the $\vec{V} \times \vec{B}$ and IOL. Γ^{Pinch}, which appears in Equation (31), is given by the expression in Equation (32).

$$\frac{\partial}{\partial r}\left(D_{jj}\frac{\partial n_j}{\partial r}\right) - \frac{\partial}{\partial r}\left(D_{jk}\frac{\partial n_k}{\partial r}\right) - \frac{\partial}{\partial r}\left(D_{jj}\frac{n_j}{T_j}\frac{\partial T_j}{\partial r}\right) - \frac{\partial}{\partial r}\left(D_{jk}\frac{n_j}{T_k}\frac{\partial T_k}{\partial r}\right) + \frac{\partial \Gamma_{rj}^{pinch}}{\partial r} = S_j \tag{31}$$

$$\Gamma_{rj}^{pinch} \equiv -\frac{n_j E_\phi^A}{B_\theta} - \frac{M_{\phi j}}{e_j B_\theta} + \frac{n_j m_j \left(\nu_{jk} + \nu_{dj}\right)}{e_j B_\theta}\left(\frac{E_r}{B_\theta} + \frac{B_\phi}{B_\theta} V_{\phi j}\right) - n_j m_j \nu_{jk} V_{\phi k} \tag{32}$$

The diffusion coefficients embed the drag frequency, ν_{dj}, and the inter-species collisional frequency ν_{jk}.

$$D_{jj} \equiv \frac{m_j T_j \left(\nu_{dj} + \nu_{jk}\right)}{\left(e_j B_\theta\right)^2}, \quad D_{jk} \equiv \frac{m_j T_j \nu_{jk}}{e_j e_k B_\theta^2} \tag{33}$$

2.9 Neutral Transport

Neutrals from gas injection and gas recycling from the wall are:

- ionized by interaction with electrons, which produces
  - a plasma ion in the ion particle balance equation Equation (3) and
  - an ionization cooling term in the ion energy balance equation Equation (21); and
- interacts with a plasma ion to effectively replace a hot ion with a cool ion (charge exchange cooling term in the ion energy balance equation Equation (21)).

The transport of these neutrals are modeled using Transport Escape Probability (TEP) methodology [19, 23, 25, 13, 27, 8, 29]. The TEP physics are based on a probabilistic description of interacting and transmitting particles within a region of interest (i). The partial current, J_{ij} from a region i (note this is not indicating ions) to region j is described by Equation (34).

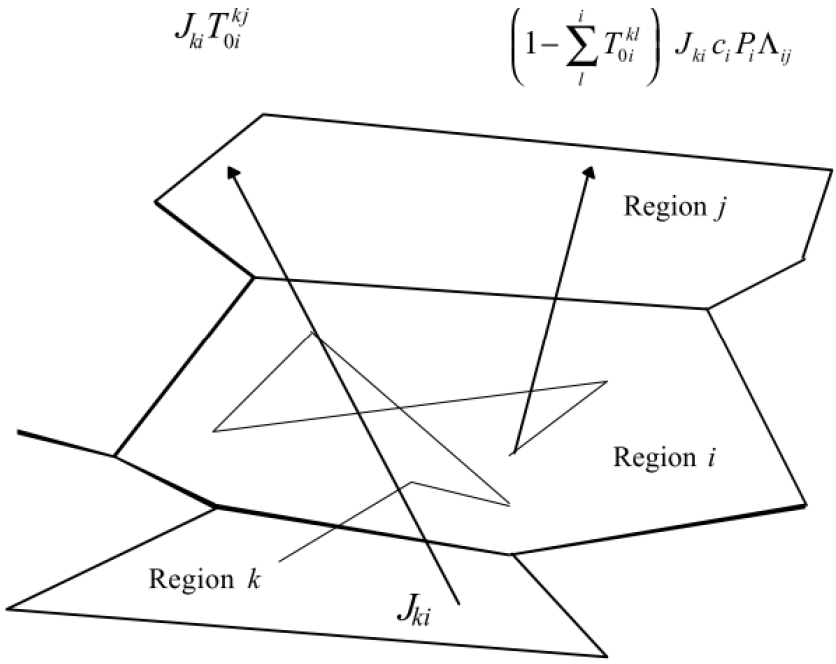

Figure 7: Transport Escape Probability (TEP) schematic diagram in 2-D geometry [13]

$$J_{ij} = \sum_{k}^{k} J_{ki}T_{0i}^{ku} + \sum_{k}^{i}\left(1 - \sum_{l}^{i} T_{0i}^{kl}\right) J_{ki}c_iP_i\Lambda_{ij} + s_iP_i\Lambda ij^s \tag{34}$$

The first term accounts for all of the partial currents entering region i (see Figure 7 on page 13) from all contiguous region k that transmit through region i. This is found by multiplying edge currents, J_{ki} by the transmission probability T_{0i}^{kj}. The second term represents all of the partial currents entering region i from contiguous regions that suffer a collision inside of region i. The collision probability is c_i, the escape probability is, P_i and the probability that scattered particles from region i escape to region j Λ_{ij}. The third term represents any internal source, such as recombination. Further description can be found in Section 2 of Rubilar, Stacey, and Mandrekas [13].

For our purposes, it has been suggested that a simplified neutral transport implementation from Stacey 2000 [23], utilizing GTNeut, should suffice. The simplified model breaks the plasma into regions shown in Figure 8 on page 14. This modeling approach will be utilized initially and modified as needed.

3 Computational Modeling

Identifying the appropriate computational approach to solving a system of equations begins with a characterization of the equations. Often this can be a daunting exercise for complex models and sub-models, as is the case with this problem. The first observation about our system of equations is that they all are one dimensional in the radial direction except for the IOL model. IOL necessarily requires a poloidal consideration, which makes this model a 1.5 dimensional model. From there, the equations generally fall into two categories, either partial first order, non-linear, differential equations or algebraic. Table 2 on page 14 shows the differential equations and their categorization while Table 3 on page 14 lists the algebraic ones. Because the equations are non-linear, the solution algorithms must be iterative in nature. The primary solver that will be explored is the Broyden solver, which is a variant within the family of Newton-Raphson solvers. The solver is discussed in 3.2.

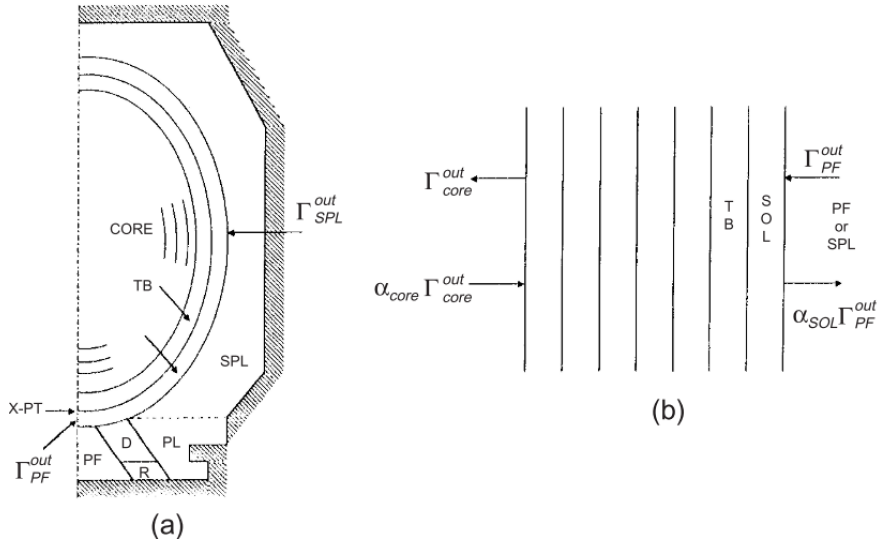

Figure 8: Schematic diagram of the neutral transport model: (a) 2-D TEP model of divertor plasma (D), recycling region (R), private flux (PF), plenum (PL) and SOL plenum (SPL); (b) 1-D ICB model of penetration through SOL and transport barrier (TB) into core. [23]

Table 2: Categorization of Differential Equations

Equation	Number	Order	Type	Reason
Particle Conservation	3	1st	Non-linear	IOL Coefficient on Γ is a function of Γ vicariously through the Temperature
Energy	21 & 22	1st	Non-linear	IOL Coefficient on Γ is a function of Γ vicariously through the Temperature
Conduction Closure	23 & 24	1st	Non-linear	Temperature multiplied by Γ

Table 3: List of Algebraic Equations

Equation	Number
Minimum Energy	11 & 12
Radial Momentum	18
Toroidal Momentum	19
Poloidal Momentum	20
Beam Cross-section	27

3.1 Iteration Strategy

The iteration strategy requires that consideration be made for calculation order. Identifying what parameters to initialize and which ones to solve for require thought. From the initial guessed parameters, the sequence of calculations should progress in such a way that all subsequent equations have the necessary input to avoid the nefarious "use-before-calculate". The flow chart in Figure 9 on page 17 shows the iteration strategy chosen. The easiest way to understand the chart is to begin with the error term ΔT_i. Essentially, there are two manners by which to arrive at the ion temperature. The upper half of the flow-map utilizes an initial guess of densities, both primary ion and impurity as well as electron temperature, to source the conservation of momentum and the Beam Cross-section/Deposition calculations. Combining these with the results of the Particle conservation results in a calculation of pressure which then implies a temperature through the ideal gas law.

The second path on the lower half of the flow chart determines a temperature by way of a thermal IOL and a fast IOL calculation, which then feeds the conservation of energy and conduction closure equations. This results in a separate temperature. The iteration then proceeds from the error in ion temperature. The solver, of which ever flavor eventually chosen, must intelligently update the primary ion density until a solution is found.

The impurity density in this iteration strategy is assumed to be specified, since this study does not consider mechanisms of impurity source generation.

It is also worth noting that the conservation of momentum calculation was ordered the way that it is, because the poloidal and toroidal momentum equations have:

- calculated particle flux, Γ from particle conservation,
- toroidal E_{φ}^{A} and poloidal E_{θ}^{A} electric fields, which are user specified,
- calculated IOL momentum contributions, and
- user specified NBI momentum contributions

3.2 Solver Selection

Algebraic solvers, such as Gauss-Jordan reduction, are applicable to predictive calculations where the densities and temperatures are sourced by experimental data, but they are not applicable to boundary valued iterative problems. Of the solvers that appropriate for iterative techniques, several but were considered and dismissed. Generalized Minimal Residual Method (GMRES) style solvers are appropriate for a non-symmetric system of linear equations [4]. Our equations are non-linear. Pure Newton Methods were dismissed because they require analytic functions so that the Jacobian can be analytically calculated. Our equations do not have an obvious analytic form. That leaves us with quasi Newton-Raphson methods in which the Jacobian is calculated computationally. The most widely used quasi Newton-Raphson method is the Broyden method. The Broyden method approaches the rate of convergence of a pure Newton-Raphson method, however, it accomplishes this at a fraction of the computational cost because the full Jacobian is not recalculated, but is evaluated numerically and algorithmically updated in subsequent iterations.

The update of values from iteration to iteration follows a similar approach to Newton's methods (Equation (35)), namely:

$$x_{+} = x_{c} - B_{c}^{-1} F(x_{c}). \tag{35}$$

This nomenclature is directly borrow from reference [4]. The subscript c indicates current values, whereas the + refers to updated values. F is the function being evaluated, and B is the Broyden matrix which is the numerical analogue of the analytic Jacobian. In pure Newton's methods, the Jacobian would be recalculated for each successive iteration. However, Broyden's method utilizes a secant update approach given by Equation (36)

Table 4: Some Selected Shots for Validation

Shot Type	Shot Number	Time (ms)
L-Mode	144567	4000
H-Mode	161409	5000
SH-Mode	171322	1800
RMP	161409	5600
NT-Mode	179990	1400

$$B_+ = B_c + \frac{(y - B_c\, s)s^T)}{s^T s} = B_c + \frac{F(x_+)s^T}{s^T s} \quad \text{where } y = F(x_+) - F(x_c) \text{ and } s = x_+ - x_c \tag{36}$$

One last thing should be noted. It is unknown at this point how non-linear the system of equations are. If the IOL proves to not be sensitive to changes in temperature, then it might be possible to revisit other iterative techniques such as GMRES.

4 Validation

The model must be validated against a variety of plasma modes. The parameters of interest include both carbon and electron densities and temperatures, as well as rotation velocities/frequencies. Some of the important modes to consider include:

- L-Mode,
- H-Mode,
- SH-Mode,
- RMP, and
- NT-Mode

Test data showing various profiles have been presented to illustrate some of the differences in profile behavior that needs to be modeled. Carbon and electron temperature are illustrated in Figure 10 on page 19 and Figure 11 on page 20, respectively, while their densities are shown in Figure 12 on page 21 and Figure 13 on page 22, respectively. Finally, available rotation data for several shots are presented in Figure 14 on page 23. Some shots show steep gradients while others less so. Rather than presenting a detailed comparison of features in the presented data set, what is relevant for this research is that hope of this methodology is to successfully reproduce curvatures and gradients exhibited in the test data.

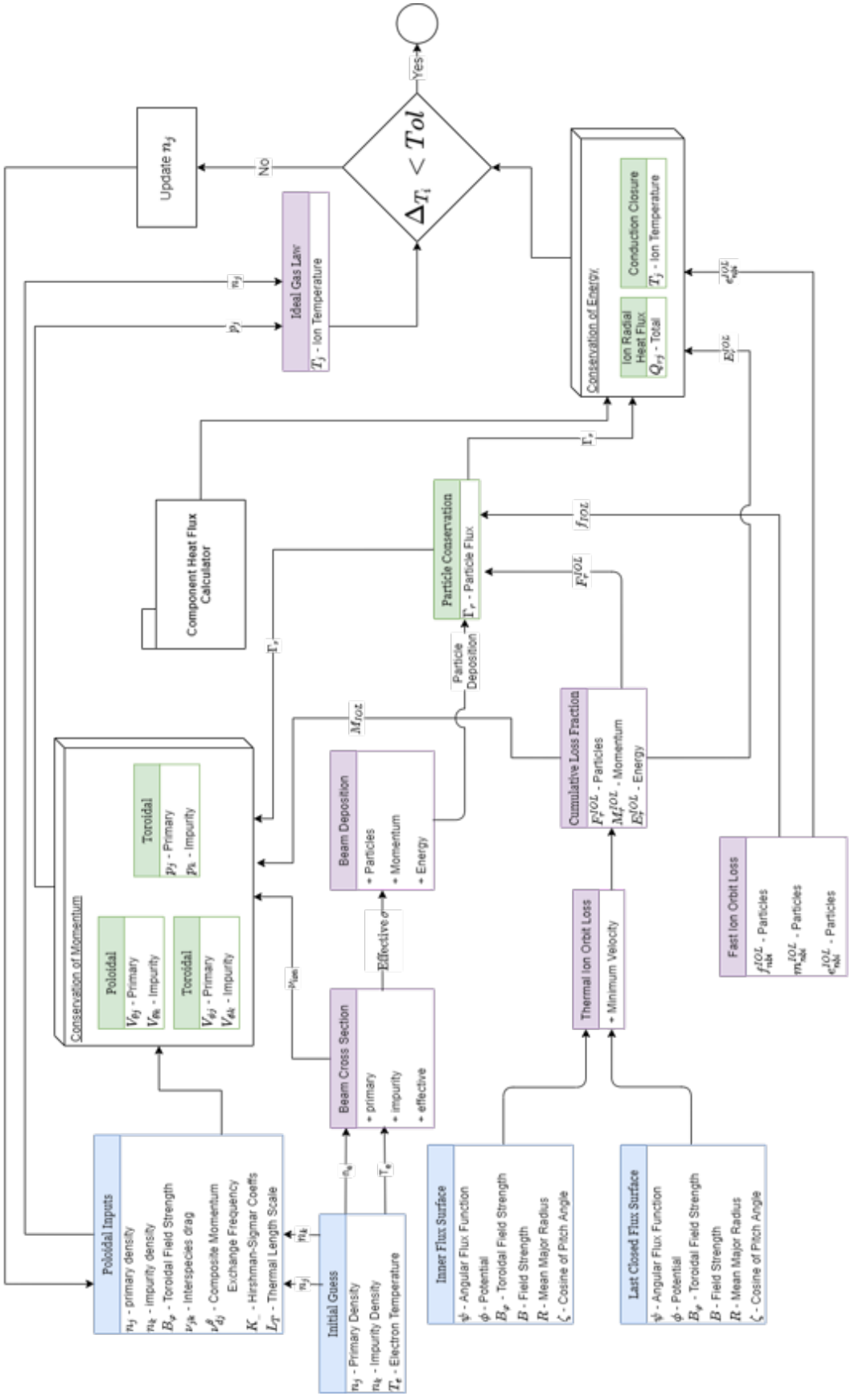

Figure 9: Iteration Strategy Flow Chart

5 Timeline

The following success oriented schedule is the optimistic timeline.

- Model Development (Duration 2.5 Months - Aug 13, 2021)
  - Refactoring of Beam Deposition code
  - Refactoring of the Ion Orbit Loss code
  - De-bugging the python implementation of GTNeut
  - Implementation of:
    - Momentum Conservation Equations
    - Energy Balance Equations
    - Solver
  - Development of the Pinch Diffusion model
- Validation (Duration 1.5 Months - Oct 29, 2021)
  - Periodic Evaluation of Sub-models
  - Final Comparison against test data
- Writing (Duration 1 Month - Nov 26, 2021)
  - Periodic Writing
  - Rough Draft
- Defense December 2

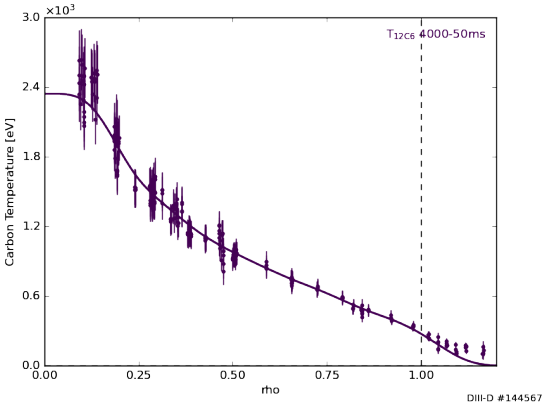

(a) L-Mode 144567_4000

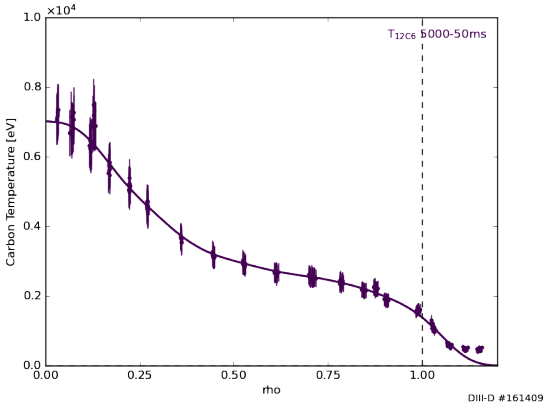

(b) H-Mode Shot:161409_5000

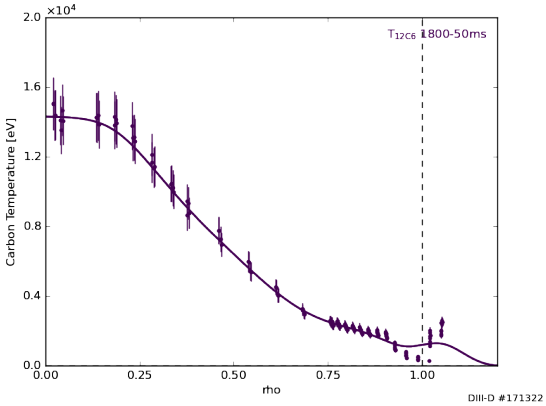

(c) SH-Mode Shot:171322_1800

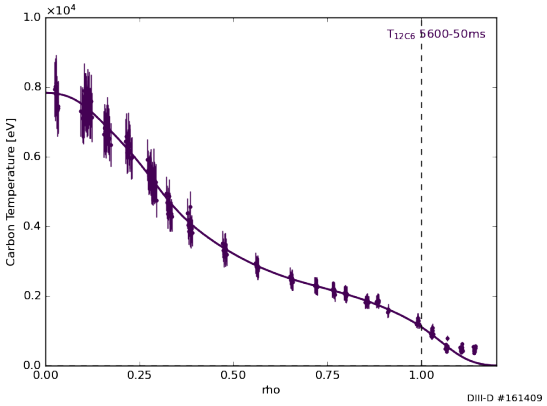

(d) RMP Shot:161409_5600

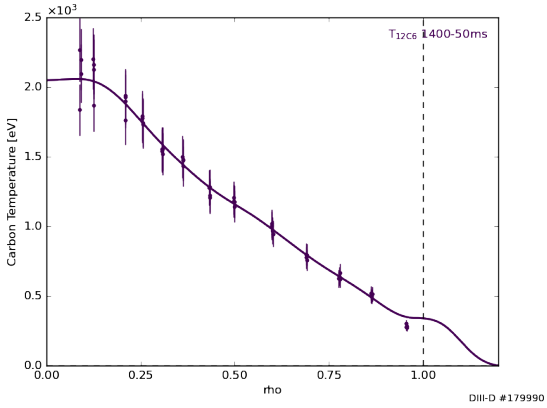

(e) NT-Mode Shot:179990_1400

Figure 10: Carbon Temperature

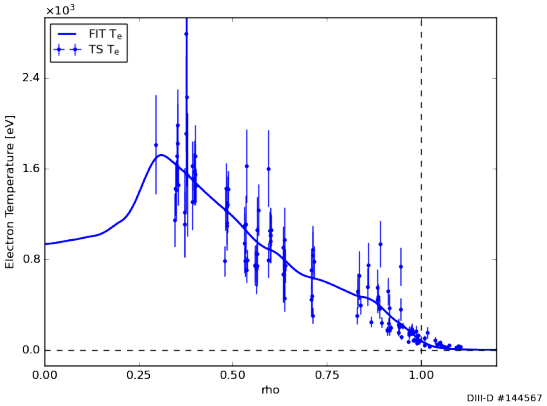

(a) L-Mode 144567_4000

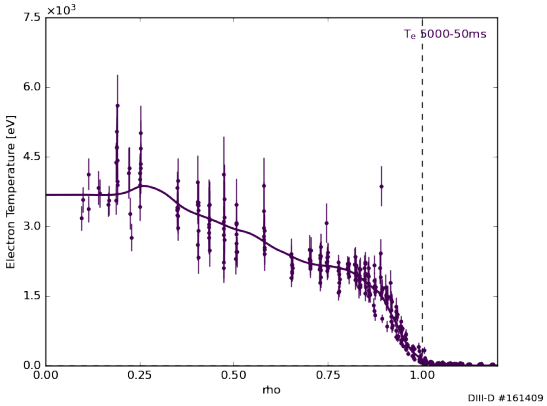

(b) H-Mode Shot:161409_5000

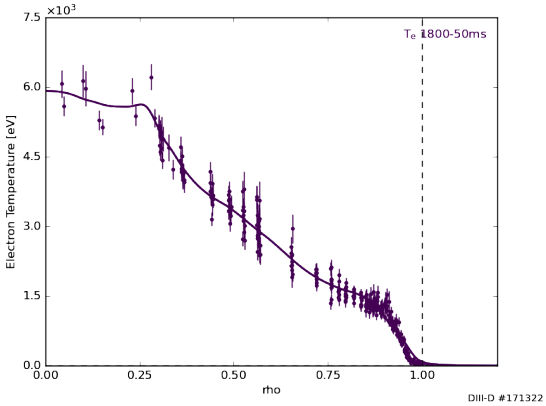

(c) SH-Mode Shot:171322_1800

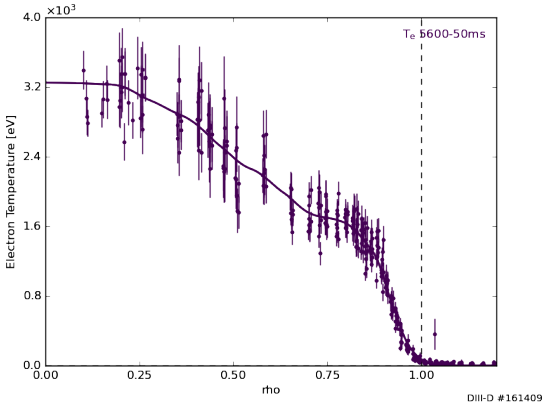

(d) RMP Shot:161409_5600

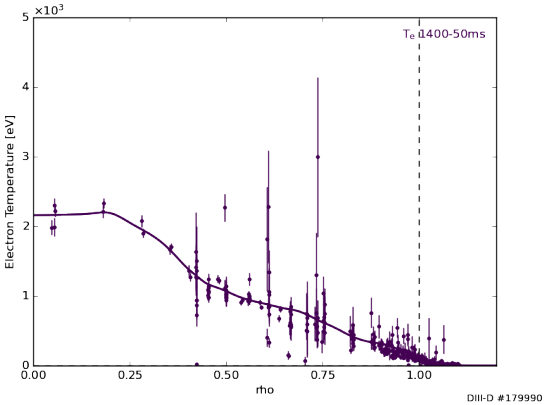

(e) NT-Mode Shot:179990_1400

Figure 11: Electron Temperature

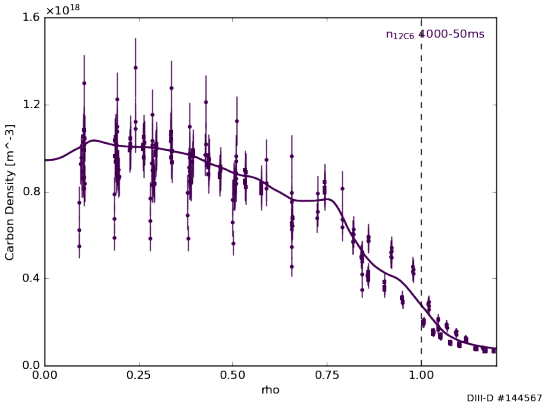

(a) L-Mode 144567_4000

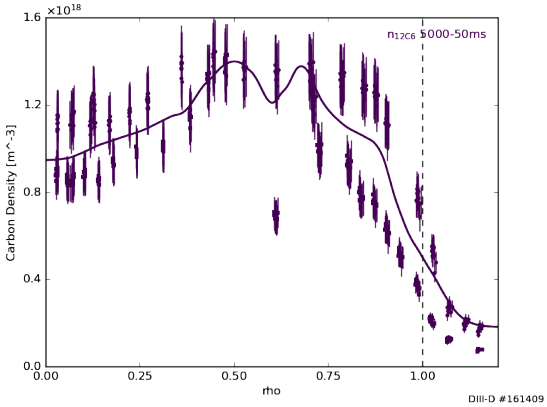

(b) H-Mode Shot:161409_5000

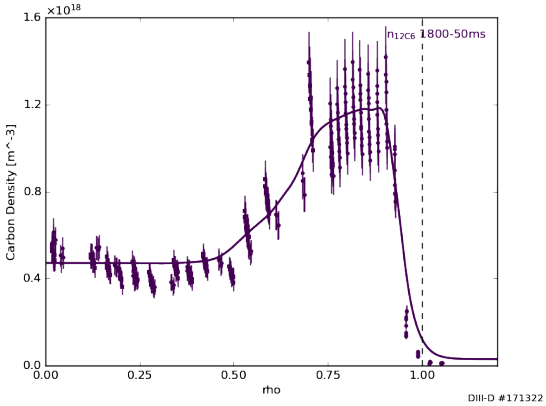

(c) SH-Mode Shot:171322_1800

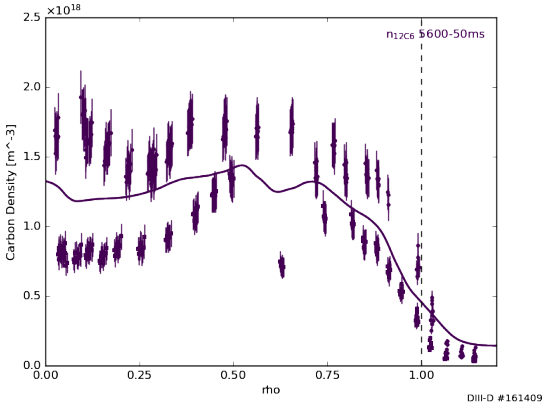

(d) RMP Shot:161409_5600

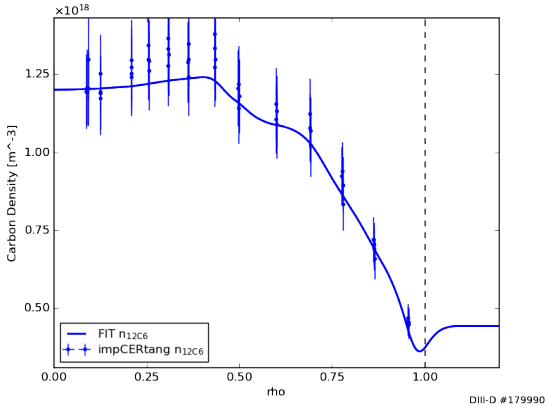

(e) NT-Mode Shot:179990_1400

Figure 12: Carbon Density

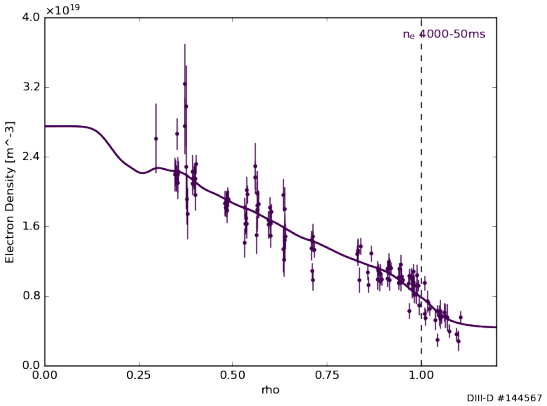

(a) L-Mode 144567_4000

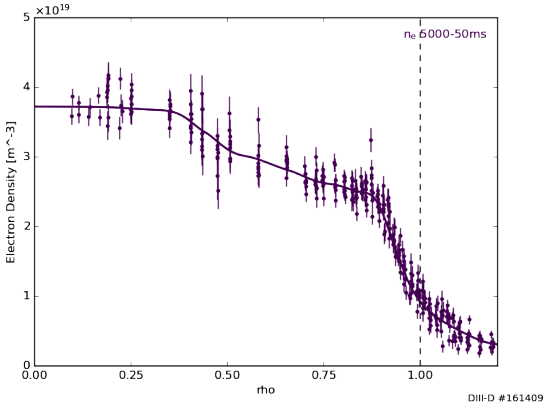

(b) H-Mode Shot:161409_5000

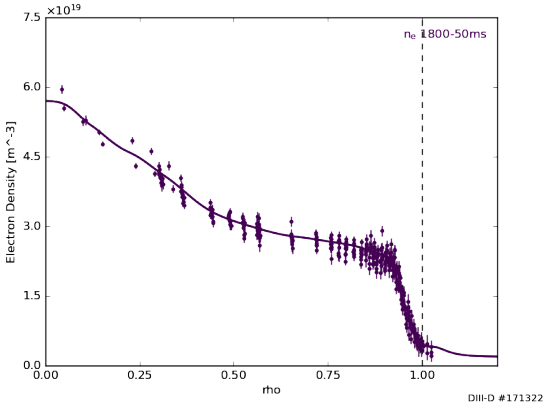

(c) SH-Mode Shot:171322_1800

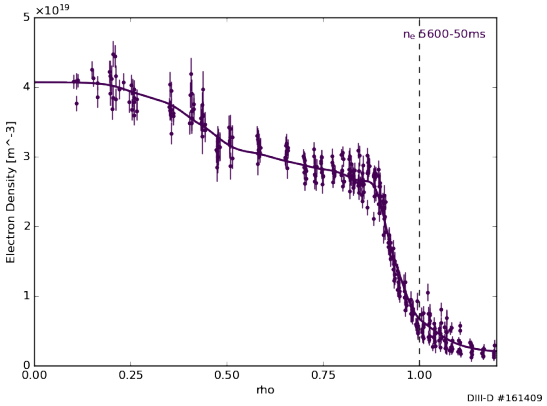

(d) RMP Shot:161409_5600

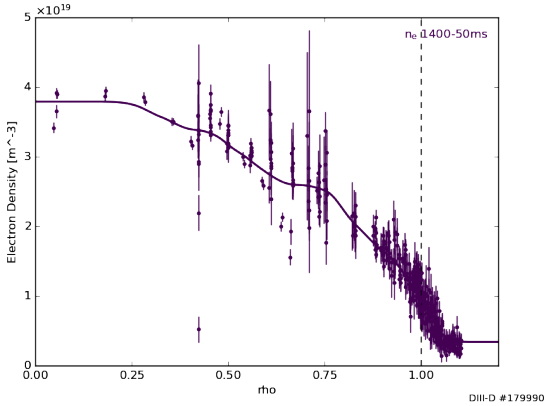

(e) NT-Mode Shot:179990_1400

Figure 13: Electron Density

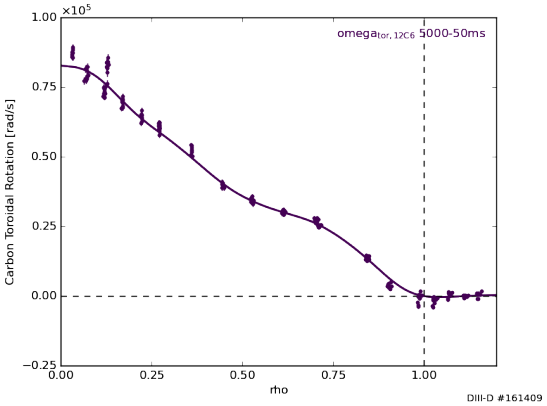

(a) H-Mode Shot:161409_5000

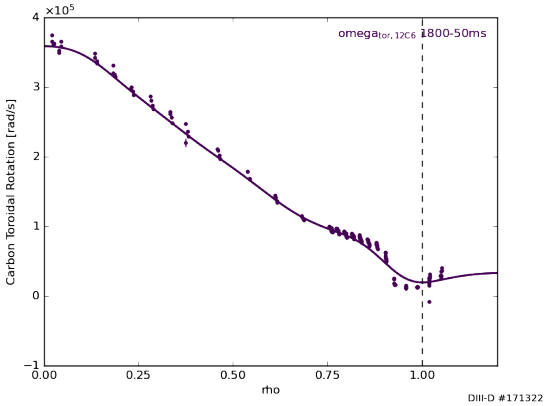

(b) SH-Mode Shot:171322_1800

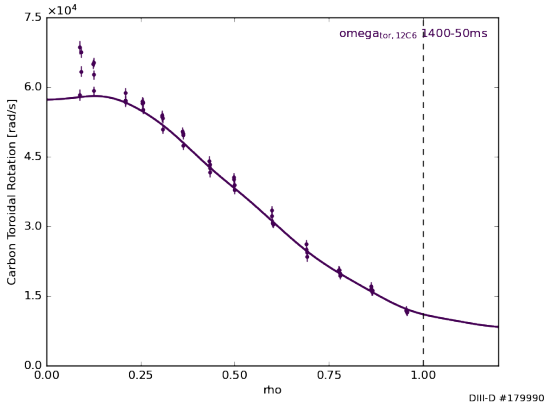

(c) NT-Mode Shot:179990_1400

Figure 14: Toroidal Rotation

Nomenclature

Parameters

α, β	Charge neutrality adjustment term	
$\hat{\alpha}$	description	
$\hat{\Gamma}$	Radial flux	$\frac{1}{s \cdot sr}$
ν_{ion}	Frequency of Ionization	
F^{IOL}	Thermal Ion Orbit Loss fraction	
f^{IOL}	Fast Ion Orbit Loss fraction	
L_p^{-1}	Pressure Gradient Scale Length $\frac{1}{p}\frac{\partial p}{\partial r}$	
L_T^{-1}	Temperature Gradient Scale Length $\frac{1}{T}\frac{\partial T}{\partial r}$	
n	Species number density	
N_{nb}	Fast Neutral Beam Source Rate	
r	Radial location along the minor radius	
S_n	Particle source	
z	Atomic Number	

Subscripts

e	Electron
j	Primary Ion
k	Impurity Ion
r	Radial Component
nbi	Neutral Beam Injection

Glossary

H-Mode Short for High Mode, an operational regime characterized by a steep pressure, density, and temperature pedestal. 1, 3

L-Mode Short for Low Mode, an operational regime characterized by a shallow pressure, density, and temperature pedestal. 3

NT-Mode Short for Negative Triangularity Mode, an operational regime characterized by a D-shaped cross-section that points radially inward (major axis) rather than the more common radially outward facing D-shape. 1, 3

SH-Mode Short for Super High Modee, an operational regime with an elevated pedestal pressure relative to H-Mode. 1

SOL A region outside of the LCFS that serves as the exhaust for tokamak plasmas. It derives its name from the early tokamak designs that put a physical barrier known as a limiter in the region to "scrape" off the outer layer of the plasma. The limiter design has mostly been replaced with the divertor design but this plasma region retains the same designation.. 4

References

[1] S I Braginskii. "Transport Processes in a Plasma". In: *Reviews of plasma physics.* 2 (1965), p. 17.

[2] John-Patrick Floyd and W M Stacey. "Numerical Investigation of the Generalized Pinch-Diffusion Equations in the Edge Pedestal". In: *Fusion Science and Technology* 61.3 (2012), pp. 227–235. ISSN: 1536-1055. DOI: 10.13182/FST12-A13535. URL: https://doi.org/10.13182/FST12-A13535.

[3] R. K. Janev, C. D. Boley, and D. E. Post. "Penetration of energetic neutral beams into fusion plasmas". In: *Nuclear Fusion* 29.12 (1989), pp. 2125–2140. ISSN: 17414326. DOI: 10.1088/0029-5515/29/12/006.

[4] C. T. Kelley. "1. Basic Concepts and Stationary Iterative Methods". In: *Iterative Methods for Linear and Nonlinear Equations* (1995), pp. 3–10. DOI: 10.1137/1.9781611970944.ch1.

[5] M. Knolker et al. "Optimizing the Super H-mode pedestal to improve performance and facilitate divertor integration". In: *Physics of Plasmas* 27.10 (2020). ISSN: 10897674. DOI: 10.1063/5.0011008.

[6] L L Lao et al. "Equilibrium analysis of current profiles in tokamaks". In: *Nuclear Fusion* 30.6 (1990), pp. 1035–1049. ISSN: 0029-5515. DOI: 10.1088/0029-5515/30/6/006. URL: http://dx.doi.org/10.1088/0029-5515/30/6/006.

[7] A.; et al Loarte. *H-mode experiments in Alcator C-Mod and consequences for ITER Q DT = 10 operation High confinement / high radiated power H-mode experiments in Alcator C- Mod and consequences for ITER Q DT = 10 operation.* Tech. rep. January. Plasma Science and Fusion Center, MIT, 2011. URL: https://dspace.mit.edu/bitstream/handle/1721.1/94396/10ja054%7B%5C_%7Dfull.pdf?sequence=1.

[8] J. Mandrekas et al. "Neutral transport analysis of recent DIII-D neutral density experiments". In: *Nuclear Fusion* 43.5 (2003), pp. 314–320. ISSN: 00295515. DOI: 10.1088/0029-5515/43/5/303.

[9] John Mandrekas. "Physics models and user ' s guide for the neutral beam module of the SuperCode". In: (1992), p. 23.

[10] A Marinoni et al. "Negative Triangularity plasmas on DIII-D : a novel approach to the core-edge integration problem". In: 510.2007 (2020), p. 115001.

[11] S. Yu Medvedev et al. "The negative triangularity tokamak: Stability limits and prospects as a fusion energy system". In: *Nuclear Fusion* 55.6 (2015). ISSN: 17414326. DOI: 10.1088/0029-5515/55/6/063013.

[12] K Miyamoto. "Direct ion orbit loss near the plasma edge of a divertor tokamak in the presence of a radial electric field". In: *Nuclear Fusion* 36.7 (1996), pp. 927–938. DOI: 10.1088/0029-5515/36/7/i09. URL: http://dx.doi.org/10.1088/0029-5515/36/7/I09%20http://stacks.iop.org/0029-5515/36/i=7/a=I09.

[13] R Rubilar, W M Stacey, and J Mandrekas. "Comparison of the TEP method for neutral particle transport in the plasma edge with the Monte Carlo method". In: *Nuclear Fusion* 41.8 (2001), p. 1003. URL: http://stacks.iop.org/0029-5515/41/i=8/a=305.

[14] W M Stacey. "Edge pedestal structure". In: *Physics of Plasmas* 11.12 (2004), pp. 5487–5496. DOI: 10.1063/1.1808751.

[15] W M Stacey. "Extended fluid transport theory in the tokamak plasma edge". In: *Nuclear Fusion* 57.6 (2017), p. 66034. DOI: 10.1088/1741-4326/aa6b34.

[16] W M Stacey. "Ion Particle Transport in the Tokamak Edge Plasma". In: *Contributions to Plasma Physics* 48.1-3 (2008), pp. 94–98. DOI: 10.1002/ctpp.200810016.

[17] W M Stacey. "Particle transport and density gradient scale lengths in the edge pedestal". In: *Contributions to Plasma Physics* 44.1-3 (2004), pp. 100–104. DOI: 10.1002/ctpp.200410014. URL: https://onlinelibrary.wiley.com/doi/abs/10.1002/ctpp.200410014.

[18] W M Stacey and R J Groebner. "A framework for the development and testing of an edge pedestal model: Formulation and initial comparison with DIII-D data". In: *Physics of Plasmas* 10.6 (2003), pp. 2412–2421. DOI: 10.1063/1.1575233. URL: https://doi.org/10.1063/1.1575233.

[19] W M Stacey and J Mandrekas. "A transmission/escape probabilities model for neutral particle transport in the outer regions of a diverted tokamak". In: *Nuclear Fusion* 34.10 (1994), p. 1385. URL: http://stacks.iop.org/0029-5515/34/i=10/a=I07.

[20] W M Stacey and D J Sigmar. "Viscous effects in a collisional tokamak plasma with strong rotation". In: *The Physics of Fluids* 28.9 (1985), pp. 2800–2807. URL: https://aip.scitation.org/doi/abs/10.1063/1.865240.

[21] W M Stacey et al. "Intrinsic rotation produced by ion orbit loss and X-loss". In: *Physics of Plasmas* 19.11 (2012), p. 112503. DOI: 10.1063/1.4768424. URL: https://aip.scitation.org/doi/abs/10.1063/1.4768424.

[22] W. M. Stacey. "Effect of ion orbit loss on distribution of particle, energy and momentum sources into the tokamak scrape-off layer". In: *Nuclear Fusion* 53.6 (2013). ISSN: 00295515. DOI: 10.1088/0029-5515/53/6/063011.

[23] W. M. Stacey. "Modelling the neutral density in the edge of the DIII-D plasma". In: *Nuclear Fusion* 40.5 (2000), pp. 965–973. ISSN: 00295515. DOI: 10.1088/0029-5515/40/5/309.

[24] Weston M Stacey. "A Particle-, Momentum-, and Energy-Conserving Fluid Transport Theory for the Tokamak Plasma Edge". In: *Fusion Science and Technology* 75.4 (2019), pp. 251–263. DOI: 10.1080/15361055.2019.1574529. URL: https://doi.org/10.1080/15361055.2019.1574529.

[25] Weston M Stacey. "An edge pedestal model based on transport and atomic physics". In: *Physics of Plasmas* 8.9 (2001), pp. 4073–4079. DOI: 10.1063/1.1388175. URL: https://doi.org/10.1063/1.1388175.

[26] Weston M Stacey. "Radial Transport Fluxes and Distributions Determined by Requirements for Particle, Momentum, and Energy Conservation". In: *Fusion Science and Technology* 76.2 (2020), pp. 153–156. DOI: 10.1080/15361055.2019.1704595. URL: https://doi.org/10.1080/15361055.2019.1704595.

[27] Weston M Stacey, John Mandrekas, and Robert Rubilar. "Interface Current Integral Transport Methods for the Calculation of Neutral Atom Transport in the Edge Region of Fusion Plasmas". In: *Fusion Science and Technology* 40.1 (2001), pp. 66–78. DOI: 10.13182/FST01-A181. URL: https://doi.org/10.13182/FST01-A181.

[28] T M Wilks and W M Stacey. "Improvements to an ion orbit loss calculation in the tokamak edge". In: *Physics of Plasmas* 23.12 (2016), p. 122505. DOI: 10.1063/1.4968219. URL: http://aip.scitation.org/doi/abs/10.1063/1.4968219.

[29] Dingkang Zhang, J Mandrekas, and W M Stacey. "Higher order approximations of the transmission and escape probability method for neutral particle transport in edge plasmas". In: *Physics of Plasmas* 13.6 (2006), p. 62509. DOI: 10.1063/1.2212934. URL: https://aip.scitation.org/doi/abs/10.1063/1.2212934.